Published in final edited form as:
Nature. 2005 December 15; 438(7070): 975–980.

Probing the Structure and Electrostatics of Ion-Channel Pores One Proton at a Time

Gisela D. Cymes[1], **Ying Ni**[1], and **Claudio Grosman**[1]
1 *Department of Molecular and Integrative Physiology, Center for Biophysics and Computational Biology, and Neuroscience Program, University of Illinois at Urbana-Champaign, Urbana, IL 61801, USA.*

Abstract

Although membrane proteins often rely on ionizable residues for structure and function, their ionization states under physiological conditions largely elude experimental estimation. To gain insight into the effect of the local microenvironment on the proton affinity of ionizable residues, we engineered individual lysines, histidines, and arginines along the α-helical lining of the nicotinic-receptor's transmembrane pore. Individual proton binding/unbinding reactions were detected electrophysiologically - at the single-side-chain, single-proton level - as brief blocking/unblocking events of the passing cation current. Kinetic analysis of these fluctuations yielded the position-dependent rates of proton transfer, from which the corresponding pK_as and pK_a-shifts were calculated. Here we present a self-consistent, residue-by-residue description of the microenvironment around the pore-lining transmembrane α-helices (M2) in the open-channel conformation, in terms of the excess free-energy that is required to keep the engineered basic side chains protonated relative to bulk water. A comparison with closed-channel data leads us to propose that the rotation of M2, frequently invoked as a hallmark of the gating mechanism of Cys-loop receptors, is minimal, if any.

Electrostatic interactions play a major role in diverse aspects of protein structure and function[1–4], ranging from enzyme catalysis, ligand binding, and the fine-tuning of redox potentials, to the stability of folded proteins, and the translocon-mediated integration of transmembrane segments into the endoplasmic reticulum. These interactions often involve full charges on the side chains of ionizable amino acids that arise from the association/dissociation of protons to/from these acid-base groups in the protein. In the particular case of ion channels, charges on ionizable side chains control single-channel conductance[5,6], ion selectivity[7–9], open-channel block[10,11], gating[12], and voltage sensing[13,14]. Knowledge of the protonation state of these residues is required for a thorough understanding of these electrostatically-controlled phenomena in quantitative detail but the pK_a-values of ionizable side chains in ion channels, as well as in most other large membrane proteins, continue to elude experimental determination. Also, since the probability of these side chains bearing a charge at a given pH is a function of the electrostatic properties of the surrounding microenvironment, the well-known pK_a-values of these side chains in *bulk* solution cannot be used to predict protonation states in any but the most trivial cases (i.e., when the protonatable group is surface-exposed). Furthermore, it is well recognized that the uncertainty associated with theoretically-calculated pK_a-values increases with the extent of burial of the side chain in question[15,16], a problem that, we gather, might be even more acute in the case of membrane proteins due to the paucity of experimentally-estimated benchmark values.

Correspondence and requests for materials should be addressed to C.G. (grosman@life.uiuc.edu)..

Supplementary Information is linked to the online version of the paper at **www.nature.com/nature**.

Single-side-chain acid-base titrations

We reasoned that, due to their unique properties, ion channels provide an extraordinary opportunity to investigate the effect of the protein microenvironment on the (time-averaged) pK_as of ionizable residues located within pore domains. In principle, individual protonation/deprotonation events, which would cause the net charge of the pore to oscillate by one unit, should be evident in a single-channel recording as current fluctuations between two levels, one corresponding to the 'neutral' pore, and the other one corresponding to the pore carrying the extra unit charge. For instance, in the case of a single basic residue (i.e., lysine, arginine, or histidine) engineered in a cation-selective pore, the 'deprotonated channel' is expected to have roughly the same conductance as the wild-type protein, whereas the channel with the protonated residue (i.e., positively-charged) is expected to conduct cations at a somewhat lower rate. Protonation/deprotonation events occurring while the channel is open should thus be manifest as oscillations of the current between two discrete values. The ratio between these two levels would be a measure of the proximity of the protonatable group to the pore's long axis, and the kinetics of the current fluctuations would reflect directly the rates of proton transfer and the side-chain's pK_a.

That these individual proton-transfer events can actually be detected is, of course, not a foregone conclusion. The rates of proton binding and unbinding might be too fast, for example, exceeding the temporal resolution of existing single-channel recording techniques (a few microseconds under optimal conditions[17]). Alternatively, the extent to which a charge added to the pore affects the channel's conductance might be too small for any proton-transfer event to be detected as a discrete step-change in the current. Even more elementarily, since buried charges can reduce the stability of folded proteins[18], engineered ionizable side chains could prevent the correct folding and insertion of the protein into the membrane. The literature on ion channels, however, contains at least two cases for which this phenomenon has indeed been recorded at the single-channel level, namely L-type Ca^{2+} channels[19], and cyclic nucleotide-gated (CNG) channels[20]. In these two cases, the relevant ionizable groups corresponded to the naturally-occurring rings of four acidic residues present in the P-loop region of these ion channels. Although proton-transfer rates were measurable (these were exceedingly fast in aqueous solutions but were slowed down to measurable levels by changing the solvent to deuterium oxide), the protonation/deprotonation of the individual carboxylate/carboxylic groups could not be identified. Rather, the four acidic side chains seemed to somehow interact to form a single (Ca^{2+} channel) or two (CNG channel) proton-binding sites.

Engineering ionizable side chains

As a step toward understanding the effect of the microenvironment on the pK_a-values of membrane-protein residues, we systematically engineered protonatable side chains into the pore domain of the adult-type muscle nicotinic acetylcholine receptor (AChR), a member of the Cys-loop receptor superfamily of neurotransmitter-gated ion channels (Fig. 1a and Supplementary Fig. 1). This receptor offers a number of technical advantages for this sort of study, including a large conductance (~84 pS), the presence of a single copy of three of its four different subunits, and an invariant stoichiometry ($(\alpha_1)_2\beta_1\delta\varepsilon$). In this superfamily of pentameric receptor-channels, the pore is formed by the lateral association of five α-helical transmembrane segments (M2; Ref. 21), the rotation of which has been hypothesized to underlie the closed $\rightleftharpoons$ open transition[22–24]. Acidic and basic residues flank the M2 segments of all the members of the Cys-loop superfamily where, in addition to having topogenic effects that are common to all transmembrane segments, they are critical determinants of charge-selectivity, conductance, and rectification[5,9,25]. In marked contrast, protonatable residues are very rare *within* the membrane-spanning portion of M2 in these channels, being completely absent in the particular case of nicotinic receptors. Although protonation states for some of these naturally-occurring

residues have been suggested on the basis of electrostatic-model calculations[26], the need for experimental approaches is obvious.

First, we introduced single lysines, one at a time, into a continuous stretch of 32 residues of the AChR's δ subunit starting with Pro 250 (−7' position; Fig. 1a), at the N-terminal end of the M1-M2 loop, and ending with Thr 281 (25' position), close to the C-terminal end of the extracellular portion of the M2 helix. The naturally-occurring lysines occupying positions 0' and 20' (Fig. 1a) were mutated to alanine, whereas Asp -5', Glu -1', and Arg 21' were mutated to both alanine and lysine. All constructs were successfully expressed in HEK-293 cells, and the current-blocking effect of single protonated lysines was indeed observed, and analyzed in detail. Figure 1b-d summarizes the effect of the $\varepsilon NH_2/NH_3^+$ group of lysine on the AChR's single-channel conductance. Insofar as the extent of channel block (Fig. 1d) can be taken as an approximate measure of distance between the engineered charges and the pore's long axis, this plot can be interpreted in structural terms. Thus, an uninterrupted α-helical pattern is apparent between positions 1' and 17' (perhaps even between −2' and 18'), with the narrowest constriction being formed by positions −2' and −1', and with the electrostatic effect of positive unit charges on the permeating cations decreasing steeply outside the presumed membrane-spanning region. Figure 1d also suggests a particular rotational angle for the M2 α-helix in the open-channel conformation. Positions −2', −1', 2', 6', 9', 13', and 16' appear to form the lumen-facing side of the α-helix in the open state, as lysine substitutions have their greatest blocking effect when engineered at these locations. The orientation of the other residues can be similarly inferred from this plot. The secondary structure of M2 beyond the stretch between, approximately, −4' and 18' could not be ascertained because the blocking effect of engineered charges becomes vanishingly small.

On the basis of whether protonation/deprotonation events of the introduced single lysines could be observed as fluctuations of the open-channel current between two levels of different conductance (Figs 1b and 2a), all probed positions were classified in three groups: a) the open-channel current appears to be fixed at a lower-than-wild-type conductance level at all pH-values tested (6.0, 7.4, and 9.0), with excursions to a higher-conductance level becoming somewhat more apparent, yet remaining marginally quantifiable, as the pH is raised, b) the open-channel current fluctuates between a wild-type-like ('main') and a lower-conductance ('sub-') level in a pH-dependent manner, with the occupancy of the main level increasing as the pH increases, and c) the open-channel current appears to remain fixed at, or very close to, the wild-type level at all pH-values tested (6.0, 7.4, and 9.0). Positions −2', −1', 2', 6', 9', 13', 16', 17', 18', 19', and 20' fall into the first group (circles in Fig. 1d). The reduced conductance and the failure to detect open-channel current fluctuations are consistent with the introduced lysines being predominantly protonated, whereas the pH insensitivity in the 6.0 – 9.0 pH range (Fig. 3a) suggests that the pK_a-values are high, as high or perhaps even higher than that of the lysine side chain in bulk water (~10.4). Hence, precise pK_a-values could not be estimated at these positions using the εNH_2 group of lysine as a probe. Positions −4', 1', 3', 5', 7', 8', 10', 11', 12', 14', and 15' fall into the second group (triangles in Fig. 1d). The observed pH-dependence of the main-level ⇌ sublevel current fluctuations (Fig. 3c) is compelling evidence that this phenomenon results from the protonation/deprotonation of individual lysine side chains. The mere fact that proton-transfer events involving lysines ($pK_{a,\,bulk} \cong 10.4$) can be observed indicates that the local microenvironment around these positions lowers the pK_a of the εNH_2 group, bringing it closer to the 6.0 – 9.0 pH range used in the experiments. From the estimated rates of proton association and dissociation, we calculated the side-chain pK_a-values at all these locations (Fig. 2 and Table 1; see also Supplementary Figs 2 and 3c, d, and Supplementary Methods), with the exception of positions −4', 5', and 15', in which cases the current fluctuations were difficult to resolve. Positions −7', −6', −5', 0', 4', and the continuous stretch from 21' to 25' fall into the third group (squares in Fig. 1d). A wild-type-like conductance and the absence of open-channel current fluctuations are consistent with a very acidic pK_a for the

lysine side chain, such that the probability of being protonated, and hence of blocking the cation current, is negligibly small. However, this behavior is also consistent with an orientation (e.g., large distance from the pore's axis) and/or a local microenvironment (e.g., water with bulk-like properties) that markedly screen the effect of the εNH_3^+ charge on the passing current, such that protonation/deprotonation events would go undetected even if they occurred. These two quite different scenarios, namely, a highly-downshifted pK_a or an attenuated electrostatic effect, cannot be distinguished easily on the basis of our data. We favor the notion that the latter might be the case for positions −7', −6', and −5', located on the distal end of the cytoplasmic M1–M2 linker, and for the stretch between 21' and 25' located on the portion of M2 that protrudes above the membrane into the extracellular space[23]. The situation of positions 0' and 4' is less obvious, though. If one assumed that the periodicity of the blocking effect (Fig. 1d) should be maintained without interruption throughout the α-helical segment, then a highly-depressed pK_a-value can explain the failure of these two lysines to block the current. If this were the case, then the red-square symbols in Fig. 1d show the approximate extent of channel block that *protonated* lysines at 0' and 4' would cause. On the other hand, we cannot dismiss the possibility that, due to the long (~8 Å) and flexible side chain of lysine, the 0' and 4' εNH_2 groups reach into the bulk-like intracellular water and become protonated, in a process akin to the 'snorkeling' of lysines and arginines located at the ends of lipid-embedded α-helices[27]. The screening of the εNH_3^+ charge by the highly-polarizable environment would, thus, account for the lack of observable block. However, the finding that lysines at positions 1' and 3' do not appear to 'snorkel' (i.e., their extent-of-block values are not zero; Fig. 1d), even when residing in rather hydrophobic microenvironments (Fig. 2b, c and Table 1), reduces the likelihood of the 'snorkeling' scenario. This seems particularly true for the 4'position, which is located more deeply into the membrane. Clearly, more experiments and electrostatic calculations are needed to settle this point.

To extend our pK_a measurements to locations where the introduced lysine side chains appeared to be permanently protonated, we engineered histidines at positions −2', −1', 2', 6', 9', 13', 16', and 17' (positions 18', 19', and 20' were not further investigated because the small extent of block (Fig. 1d) renders the analysis unreliable). Since the 'macroscopic' pK_a of the imidazole ring of histidine in bulk solution is ~6.4, the imidazole $\rightleftharpoons$ imidazolium$^+$ interconversion should be detected at these 'bulk-like' positions in the 6.0 – 9.0 pH range. Indeed, pH-dependent main-level $\rightleftharpoons$ sublevel fluctuations (Fig. 3b) were recorded for all of these mutants, and the corresponding pK_a-values were calculated from the kinetics of proton transfer (Fig. 2 and Table 1; see also Supplementary Figs 2 and 3a, b, and Supplementary Methods). As qualitatively expected from the corresponding lysine substitutions, the imidazole pK_as are not depressed, consistent with these positions facing the aqueous lumen of the permeation pathway. In fact, at most of these positions, the pK_as are higher than the bulk value of 6.4, which indicates that it is actually easier to charge a histidine in this location within the pore than in bulk water. Provided this is also the case for the εNH_2 group of lysine, this explains our, initially puzzling, observation that the subconductance levels of lysine constructs at these positions were oblivious to pH, even (as was the case for the 6' and 9' substitutions) when exposed to pH-values as high as 10.5. We also introduced histidines at −4', 5', and 15', three positions where lysine-induced current fluctuations were observed, but were difficult to quantify reliably. The corresponding histidine-pK_as and rates of proton transfer are included in Table 1. Finally, we also engineered a histidine in 12'. The local microenvironment around this position lowers the affinity of the lysine side chain for protons by a factor of ~30 relative to that in bulk water ($\Delta pK_a \cong 8.9 - 10.4 = -1.5$; Fig. 2 and Table 1). Thus, to the extent that the side chains of histidine and lysine probe similar microenvironments, and that their pK_as have similar sensitivities to them, a histidine in 12' is expected to be mostly deprotonated ($pK_a \cong 6.4 - 1.5 = 4.9$), even at pH = 6.0. Indeed, our single-channel recordings clearly confirmed this prediction (Fig. 3d), and we generalize this result to suggest that histidines engineered at positions that

lower the lysine's pK_a to the same or greater degree than position 12' ($\Delta pK_a < -1.5$ units; see color code in Fig. 2b, c) would be largely neutral, even at pH = 6.0.

To gain further insight into the unique microenvironment around positions 0' and 4', we engineered arginines at these positions. As was the case for the 0' and 4' lysine constructs, arginine substitutions at these two positions failed to reduce the single-channel conductance. This result confirms the notion that charging the pore at these two positions might be energetically costly (see above), to the extent that not even the guanidine group of arginine, with a bulk pK_a of ~12.0, can bind a proton at pH = 6.0. We conclude that the pK_a-shift would be of, at least, −7 units (Fig. 2 and Table 1). For comparison, we also engineered an arginine in 11' (on the same face of the α-helix as 0' and 4'), a position where lysine is predominantly deprotonated (p$K_a \cong 5.3$; Fig. 2), and where proton binding/unbinding events take place most slowly (Table 1). Although both arginine and lysine at this position block the current to similar extents (extent-of-channel-block ≅ 0.3), the 11' arginine remained charged. Excursions to a deprotonated state could not be detected, not even at pH = 9.0. Thus, we suggest that, at physiological pH, engineered arginines would keep the proton bound at all positions of the stretch between −4' and 17' with the likely exception of positions 0' and 4' (see above discussion), in which cases the arginine would be completely deprotonated, in spite of its high proton affinity in bulk water.

Figure 2 and Table 1 (see also Supplementary Fig. 2) summarize the δ-subunit pK_a results. Similar analysis on the α, β, and ε subunits (data not shown) suggests that, although with some clear differences, this general pattern of ΔpK_a-values is conserved in all four subunits.

pK_a-shifts and transfer free-energy changes

The different proton affinities of an ionizable residue in a protein and in bulk water are related, through thermodynamic cycles, to the changes in free energy associated with the transfer of the protonated *versus* deprotonated forms of the residue from bulk water to its position in the protein ($\Delta\Delta G^{\circ}_{bulk \rightarrow protein} \cong -1.36\, \Delta pK_a$ kcal/mol, at 22° C). Hence, a ΔpK_a-value is a measure of the extent to which interactions with the protein microenvironment (water molecules, protein dipoles, charges on ionizable residues) compensate for the loss of solvation free-energy incurred upon removal of the residue's charge from bulk water. Since naturally-occurring ionizable residues are only present at the ends of M2, and are absent from the membrane-spanning portions of M1, M3, and M4 (Supplementary Fig. 1a, b), the contribution of charge-charge interactions to this energetic balance is expected to be small for most positions examined here. Instead, most of the ΔpK_as reported in Fig. 2 and Table 1 are expected to be largely governed by the interactions of the positive charges on the engineered basic residues with protein dipoles (backbone dipoles, polar side chains) and water molecules in the heterogeneous environment surrounding M2. An inspection of the color-coded ΔpK_a maps in Fig. 2 suggests that the observed 'gradient' of pK_a-shifts specifically reflects the unique distribution of water molecules around the δ-subunit M2 α-helix.

The gating conformational change

In spite of significant steps toward the elucidation of the atomic-resolution structure of the full receptor[23], and toward an understanding of some general aspects of the chemical dynamics of the gating reaction[28–30], several basic aspects of the AChR still remain unsettled, such as the exact sides of the M2 α-helices that face the pore's lumen in the closed and open states[23,24,31,32], the structural rearrangements underlying the closed ⇌ open transition[23,24,33], and the locations and modes of operation of the activation[23,34] and desensitization gates. The experimental data presented here unambiguously defines the side of the δ M2 α-helix that faces the aqueous lumen of the pore in the open state (Figs 1d and 2b, c). Since our approach probes

the effect of protonation/deprotonation on single-channel conductance, the proton-transfer rates in the *closed* channel (and, by inference, the corresponding orientation of the α-helices) were not investigated here. Other approaches, however, have been utilized for the identification of residues that line the pore of the closed channel. Photoincorporation of affinity labels, for example, provided compelling evidence that residues 9', 13', and 16' face the closed-channel lumen in a muscle-type AChR[35,36]. A comparison with Figs 1d and 2b, c, thus, reveals that the inner lining of the AChR's pore is nearly the same in the closed and open states. Together, these data are consistent with a mechanism of channel opening that simply involves a widening of the pore, with the narrowest constriction switching from a location near the middle of the membrane[23] to a location near the intracellular entrance (positions −2' and −1'; Fig. 1d). The rotation of M2 is minimal, if any (see also Supplementary Discussion).

Naturally-occurring ionizable residues

The protonation state of wild-type residues is another vexing issue. Indeed, questions like the net charge of the rings of ionizable residues that flank the pore of Cys-loop receptors[37], and voltage-dependent Na^+ and Ca^{2+} channels[38], for instance, or the specific charge-stabilizing interactions that keep the pK_a of the voltage-sensing S4 arginines well above physiological pH, remain elusive. On the basis of the insight gained here, the pK_a-values of some of the native ionizable groups of the AChR, and other members of the superfamily, can be predicted (see Supplementary Discussion).

Concluding remarks

Gratifyingly, both the channel-block data (Fig. 1d) and the proton-affinity measurements (Fig. 2b, c) are remarkably consistent with one another, and with the proposed α-helical secondary structure of M2 in the closed state (Refs 23, [35, 39]). Other labeling methods have also been used to explore the properties of the AChR's open-channel pore but, because in the presence of agonist the channel interconverts rapidly among a number of different allosteric states (closed, open, and various desensitized states), labeling results can seldom be ascribed entirely to the open-channel conformation. Since identification of the open state in a single-channel record is unambiguous (Figs 1b and 3), our approach circumvents this critical problem altogether. In this paper, application of this method has allowed us to infer structural information on the AChR's open-channel pore with unprecedented detail and precision, to suggest protonation states for some of the naturally-occurring ionizable residues, to attain a deeper understanding of the pore's dielectric properties, and to provide an extensive set of highly-shifted pK_a-values, which, as the resolution of structural models of the AChR improves, could be used as meaningful benchmarks to validate theoretical electrostatic models for ion-channel proteins. More broadly, these data remind us that basic and acidic amino acids are not charged but *chargeable* residues, the pK_as of which are complex functions of the local microenvironment, and that the high energetic cost of burying the charged form of a residue, or of exposing it to lipids, can be relieved by simply releasing (basic residues) or taking (acidic ones) a proton. We anticipate that many more facets of the relationship between structure, function, and electrostatics in ion channels will be illuminated by the application of this experimental approach.

Methods

General procedures

HEK-293 cells were transiently transfected with mouse-muscle adult-type AChR cDNAs. Mutations were engineered using the QuikChange™ site-directed mutagenesis kit protocol (Stratagene), and were confirmed by dideoxy sequencing. Single-channel patch-clamp currents were recorded in the cell-attached configuration at 22º C. The bath solution was (in mM): 142

KCl, 5.4 NaCl, 1.8 $CaCl_2$, 1.7 $MgCl_2$, and 10 HEPES/KOH, pH = 7.4. The pipette solution was identical to that in the bath with the exception of the H^+-buffer, which changed depending on the desired pH of the solution. These buffers were: acetic acid/acetate (pH = 5.0), MES (pH = 6.0), HEPES (pH = 7.4), TABS (pH = 9.0), and CAPS (pH = 10.5), all titrated to final pH with KOH. The pipette solution also contained 1-μM acetylcholine (ACh).

Kinetic analysis

Protonation and deprotonation rates, as well as all other transition rates, were estimated from maximum-likelihood fitting of dwell-time series to kinetic models based on that of Fig. 2a (see Supplementary Methods for more details). To this end, we used QuB software[40,41] with a retrospectively imposed time resolution of 25 μs. At the low concentration of ACh used in the experiments described here (1 μM), only the protonation/deprotonation rates (Open → Open-H^+ and Open-H^+ → Open), and the channel-shutting rates (Open-H^+ → Shut-H^+ and Open → Shut) can be ascribed a clear physical meaning.

Supplementary Material

Refer to Web version on PubMed Central for supplementary material.

Acknowledgements

This work was supported by a grant from the National Institutes of Health to C.G. We thank S. Sine for the generous gift of wild-type muscle-AChR subunit cDNAs, J. Jasielec and J. Gasser for technical assistance, S. Varma and B. García-Moreno E. for discussions, and E. Tajkhorshid for introducing us to the VMD program.

References

1. Perutz MF. Electrostatic effects in proteins. Science 1978;201:1187–1191. [PubMed: 694508]
2. Warshel A. Electrostatic basis of structure-function correlation in proteins. Acc Chem Res 1981;14:284–290.
3. Davis ME, McCammon JA. Electrostatics in biomolecular structure and dynamics. Chem Rev 1990;90:509–521.
4. Honig B, Nicholls A. Classical electrostatics in biology and chemistry. Science 1995;268:1144–1149. [PubMed: 7761829]
5. Imoto K, et al. Rings of negatively charged amino acids determine the acetylcholine receptor channel conductance. Nature 1988;335:645–648. [PubMed: 2459620]
6. Kelley SP, Dunlop JI, Kirkness EF, Lambert JJ. A cytoplasmic region determines single-channel conductance in 5-HT_3 receptors. Nature 2003;424:321–324. [PubMed: 12867984]
7. Heinemann SH, Terlau H, Stühmer W, Imoto K, Numa S. Calcium channel characteristics conferred on the sodium channel by single mutations. Nature 1992;56:441–443. [PubMed: 1313551]
8. Yang J, Ellinor PT, Sather WA, Zhang JF, Tsien RW. Molecular determinants of Ca^{2+} selectivity and ion permeation in L-type Ca^{2+} channels. Nature 1993;366:158–161. [PubMed: 8232554]
9. Keramidas A, Moorhouse AJ, Pierce KD, Schofield PR, Barry PH. Cation-selective mutations in the M2 domain of the inhibitory glycine receptor channel reveal determinants of ion-charge selectivity. J Gen Physiol 2002;119:393–410. [PubMed: 11981020]
10. Lu Z, MacKinnon R. Electrostatic tuning of Mg^{2+} affinity in an inward-rectifier K^+ channel. Nature 1994;371:243–246. [PubMed: 7915826]
11. Khan A, Romantseva L, Lam A, Lipkind G, Fozzard HA. Role of outer ring carboxylates of the rat skeletal muscle sodium channel pore in proton block. J Physiol (London) 2002;543.1:71–84. [PubMed: 12181282]
12. Schulte U, Fakler B. Gating of inward-rectifier K^+ channels by intracellular pH. Eur J Biochem 2000;267:5837–5841. [PubMed: 10998042]
13. Aggarwal SK, MacKinnon R. Contribution of the S4 segment to gating charge in the Shaker K^+ channel. Neuron 1996;16:1169–1177. [PubMed: 8663993]

14. Seoh S–A, Sigg D, Papazian DM, Bezanilla F. Voltage-sensing residues in the S2 and S4 segments of the Shaker K^+ channel. Neuron 1996;16:1159–1167. [PubMed: 8663992]
15. Schutz CN, Warshel A. What are the dielectric "constants" of proteins and how to validate electrostatic models? Proteins 2001;44:400–417. [PubMed: 11484218]
16. Mehler EL, Fuxreiter M, Simon I, García-Moreno EB. The role of hydrophobic microenvironments in modulating pK_a shifts in proteins. Proteins 2002;48:283–292. [PubMed: 12112696]
17. Parzefall F, Wilhelm R, Heckmann M, Dudel J. Single channel currents at six microsecond resolution elicited by acetylcholine in mouse myoballs. J Physiol (London) 1998;512.1:181–188. [PubMed: 9729627]
18. Daopin S, Anderson DE, Baase WA, Dahlquist FW, Matthews BW. Structural and thermodynamic consequences of burying a charged residue within the hydrophobic core of T4 lysozyme. Biochemistry 1991;30:11521–11529. [PubMed: 1747370]
19. Prod'hom B, Pietrobon D, Hess P. Direct measurement of proton transfer rates to a group controlling the dihydropyridine-sensitive Ca^{2+} channel. Nature 1987;329:243–246. [PubMed: 2442620]
20. Root MJ, MacKinnon R. Two identical noninteracting sites in an ion channel revealed by proton transfer. Science 1994;265:1852–1856. [PubMed: 7522344]
21. Lester H. The permeation pathway of neurotransmitter-gated ion channels. Annu Rev Biophys Biomol Struct 1992;21:267–292. [PubMed: 1381975]
22. Unwin N. Acetylcholine receptor channel imaged in the open state. Nature 1995;373:37–43. [PubMed: 7800037]
23. Miyazawa A, Fujiyoshi Y, Unwin N. Structure and gating mechanism of the acetylcholine receptor pore. Nature 2003;423:949–955. [PubMed: 12827192]
24. Horenstein J, Wagner DA, Czajkowski C, Akabas MH. Protein mobility and GABA-induced conformational changes in $GABA_A$ receptor pore-lining M2 segment. Nature Neurosci 2001;4:477–485. [PubMed: 11319555]
25. Corringer PJ, et al. Mutational analysis of the charge selectivity filter of the α7 nicotinic acetylcholine receptor. Neuron 1999;22:831–843. [PubMed: 10230802]
26. Adcock C, Smith GR, Sansom MSP. Electrostatics and the ion selectivity of ligand-gated channels. Biophys J 1988;75:1211–1222. [PubMed: 9726923]
27. Stopar D, Sprujit RB, Wolfs CJ, Hemminga MA. Local dynamics of the M13 major coat protein in different membrane-mimicking systems. Biochemistry 1996;35:15467–15473. [PubMed: 8952500]
28. Grosman C, Zhou M, Auerbach A. Mapping the conformational wave of acetylcholine receptor channel gating. Nature 2000;403:773–776. [PubMed: 10693806]
29. Cymes GD, Grosman C, Auerbach A. Structure of the transition state of gating in the acetylcholine receptor channel pore: a phi-value analysis. Biochemistry 2002;41:5548–5555. [PubMed: 11969415]
30. Grosman C. Free-energy landscapes of ion-channel gating are malleable: changes in the number of bound ligands are accompanied by changes in the location of the transition state in acetylcholine-receptor channels. Biochemistry 2003;42:14977–14987. [PubMed: 14674774]
31. Goren EN, Reeves DC, Akabas MH. Loose protein packing around the extracellular half of the $GABA_A$ receptor β_1 subunit M2 channel-lining segment. J Biol Chem 2004;279:11198–11205. [PubMed: 14715650]
32. Kim S, Chamberlain AK, Bowie JU. A model of the closed form of the nicotinic acetylcholine receptor M2 channel pore. Biophys J 2004;87:792–799. [PubMed: 15298888]
33. Dahan D, et al. A fluorophore attached to nicotinic acetylcholine receptor βM2 detects productive binding of agonist to the αδsite. Proc Natl Acad Sci U S A 2004;101:10195–10200. [PubMed: 15218096]
34. Wilson GG, Karlin A. The location of the gate in the acetylcholine receptor channel. Neuron 1998;20:1269–1281. [PubMed: 9655513]
35. White BH, Cohen JB. Agonist-induced changes in the structure of the acetylcholine receptor M2 regions revealed by photoincorporation of an uncharged nicotinic noncompetitive antagonist. J Biol Chem 1992;267:15770–15783. [PubMed: 1639812]

36. Arévalo E, Chiara DC, Forman SA, Cohen JB, Miller KW. Gating-enhanced accessibility of hydrophobic sites within the transmembrane region of the nicotinic acetylcholine receptor's δsubunit. A time-resolved photolabeling study. J Biol Chem 2005;280:13631–13640. [PubMed: 15664985]

37. O'Mara M, Barry PH, Chung SH. A model of the glycine receptor deduced from Brownian dynamics. Proc Natl Acad Sci U S A 2003;100:4310–4315. [PubMed: 12649321]

38. Corry B, Vora T, Chung SH. Electrostatic basis of valence selectivity in cationic channels. Biochim Biophys Acta 2005;1711:72–86. [PubMed: 15904665]

39. Akabas MH, Kaufmann C, Archdeacon P, Karlin A. Identification of acetylcholine receptor channel–lining residues in the entire M2 segment of the alpha subunit. Neuron 1994;13:919–927. [PubMed: 7524560]

40. Qin F. Restoration of single-channel currents using the segmental k-means method based on hidden Markov modeling. Biophys J 2004;86:1488–1501. [PubMed: 14990476]

41. Qin F, Auerbach A, Sachs F. Estimating single-channel kinetic parameters from idealized patch-clamp data containing missed events. Biophys J 1996;70:264–280. [PubMed: 8770203]

42. Ohno K, et al. Congenital myasthenic syndrome caused by prolonged acetylcholine receptor channel openings due to a mutation in the M2 domain of the epsilon subunit. Proc Natl Acad Sci U S A 1995;92:758–762. [PubMed: 7531341]

43. Humphrey W, Dalke A, Schulten K. VMD: visual molecular dynamics. J Molec Graphics 1996;14:33–38.

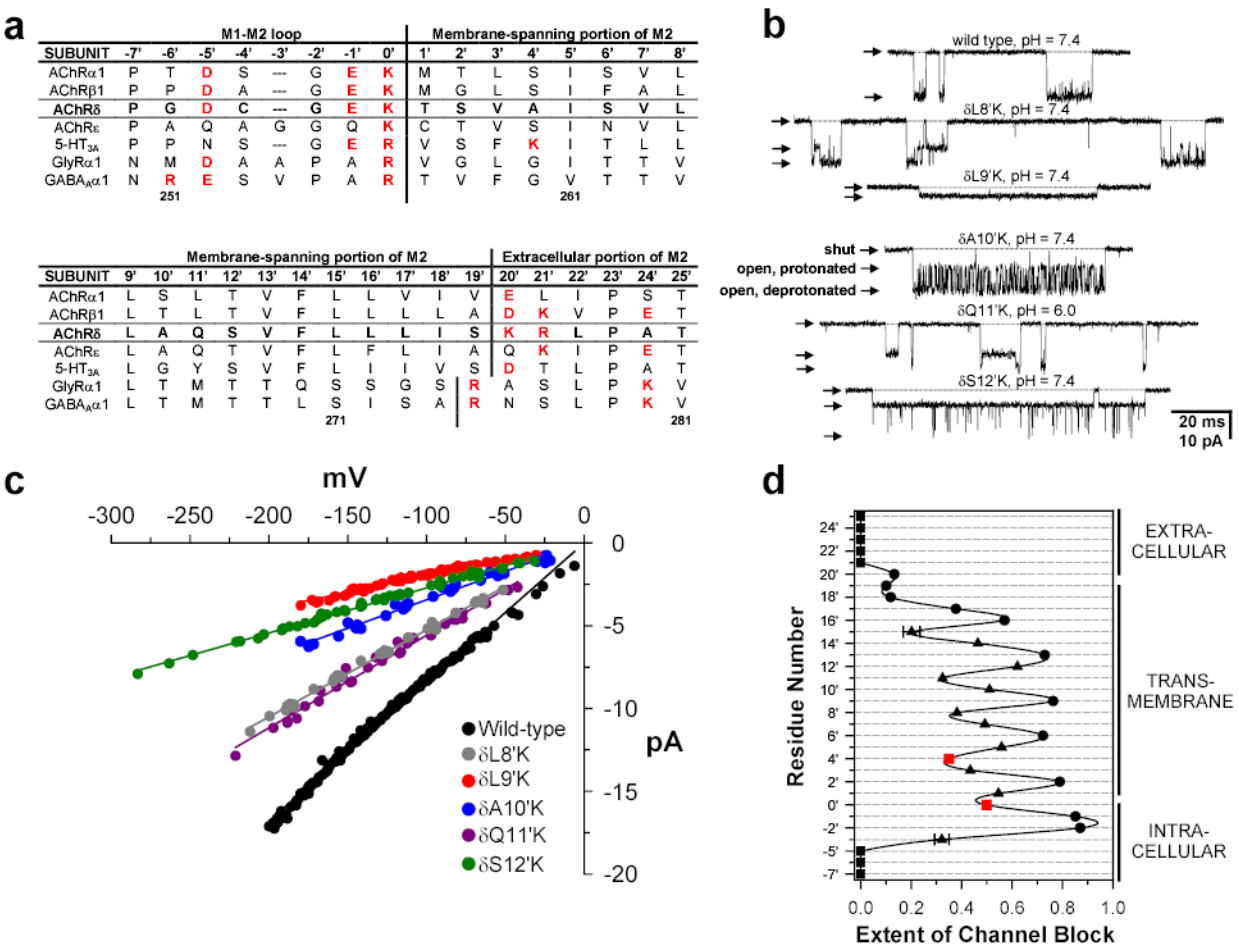

Figure 1. Protonation of lysines causes partial channel block

a, Sequence alignment corresponding to the portion of M2 studied here. The four adult mouse-muscle AChR subunits (α1, β1, δ, and ε), and one representative each of the serotonin ($5HT_3$), GABA, and glycine (GlyR) receptor-channel subunits are compared. Protonatable residues are indicated in red. AChR δ-subunit residues are indicated in bold. The prime-numbering system is indicated at the top, and the particular mouse δ-subunit residue numbers are at the bottom. **b,** Example single-channel inward currents (V ≅ −200 mV, [ACh] = 1 μM) recorded from HEK-293 cells expressing the indicated constructs. Openings are downward deflections. The shut (i.e., zero current) and the two open current-levels are indicated by arrows. The shut level of each trace is also indicated by a horizontal dotted line. Display f_c = 6 kHz. **c,** Current-voltage (I–V) relationships for the five mutants in (**b**) and the wild-type AChR. For clarity, only the I–V curve corresponding to the blocked open state is shown for each mutant. **d,** The extent of channel block for each lysine construct was calculated as the conductance difference between the main level and the sublevel, normalized by the conductance of the main level (i.e., ΔConductance/Main-Level Conductance). For positions 0' and 4', however, the extent-of-block values (red squares) are predictions based on the values observed at neighboring positions (see text and Supplementary Methods for details). The solid line is a cubic-spline interpolation. Proposed membrane boundaries[23] are tentative, and our data would not be inconsistent with these being displaced by approximately one turn toward the intracellular. Note that even residues that would be on the 'back' of the α-helix (e.g., 8', 11',

15’) exert a considerable electrostatic effect on the cation current. For most positions, the horizontal error bars (standard errors) are smaller than the experimental points. The data suggest that the pore’s lumen is to the right of the plot.

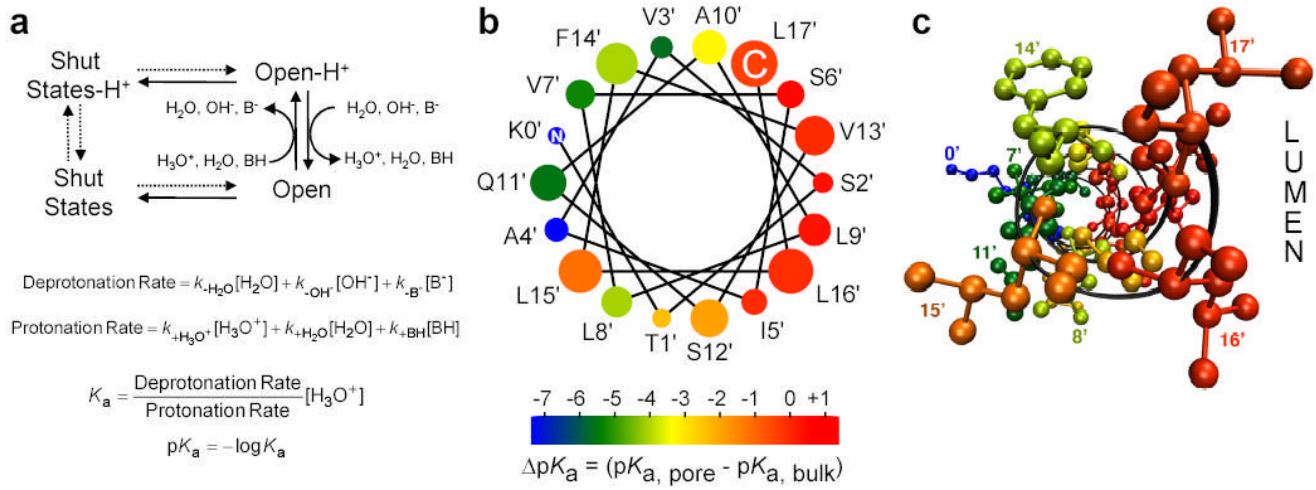

Figure 2. Experimental estimates of pK_a-values

a, Conceptual framework of this work: a simple thermodynamic cycle. The channel interconverts among closed, desensitized (both referred here, collectively, as 'shut states'), and open conformations with or without an extra proton bound to the pore domain. The association and dissociation of a single proton to the open state (but not to the shut states) is manifest as a discrete change in the rate of ion flow. Kinetic analysis of these fluctuations, and of the open ⇌ shut transitions, yields the rates of protonation and deprotonation of the open channel; these, along with the solution's pH, are then combined to calculate the engineered-residue's pK_a. The three proton donors and three proton acceptors present in the solutions are indicated. BH and B- denote the protonated and deprotonated forms of the H^+-buffer, respectively. Note that the kinetics of both proton transfer and channel shutting affect the duration of sojourns in the sub- and main levels (solid arrows). **b,** ΔpK_a-values mapped onto an ideal α-helical wheel representation of δM2. The size of the symbols increases toward the extracellular end. Wild-type residues, and the C and N ends are indicated. The pore's lumen would be to the right of the plot. The unique properties of the 15' position are discussed in the Supplementary Discussion. **c,** ΔpK_a-values mapped onto a ball-and-stick representation of the 0' – 17' δM2 stretch, using the atomic coordinates in the 1OED PDB file[23]. The color code is the same as in (**b**). The backbone is indicated in ribbon representation. The molecular image was made with VMD[43].

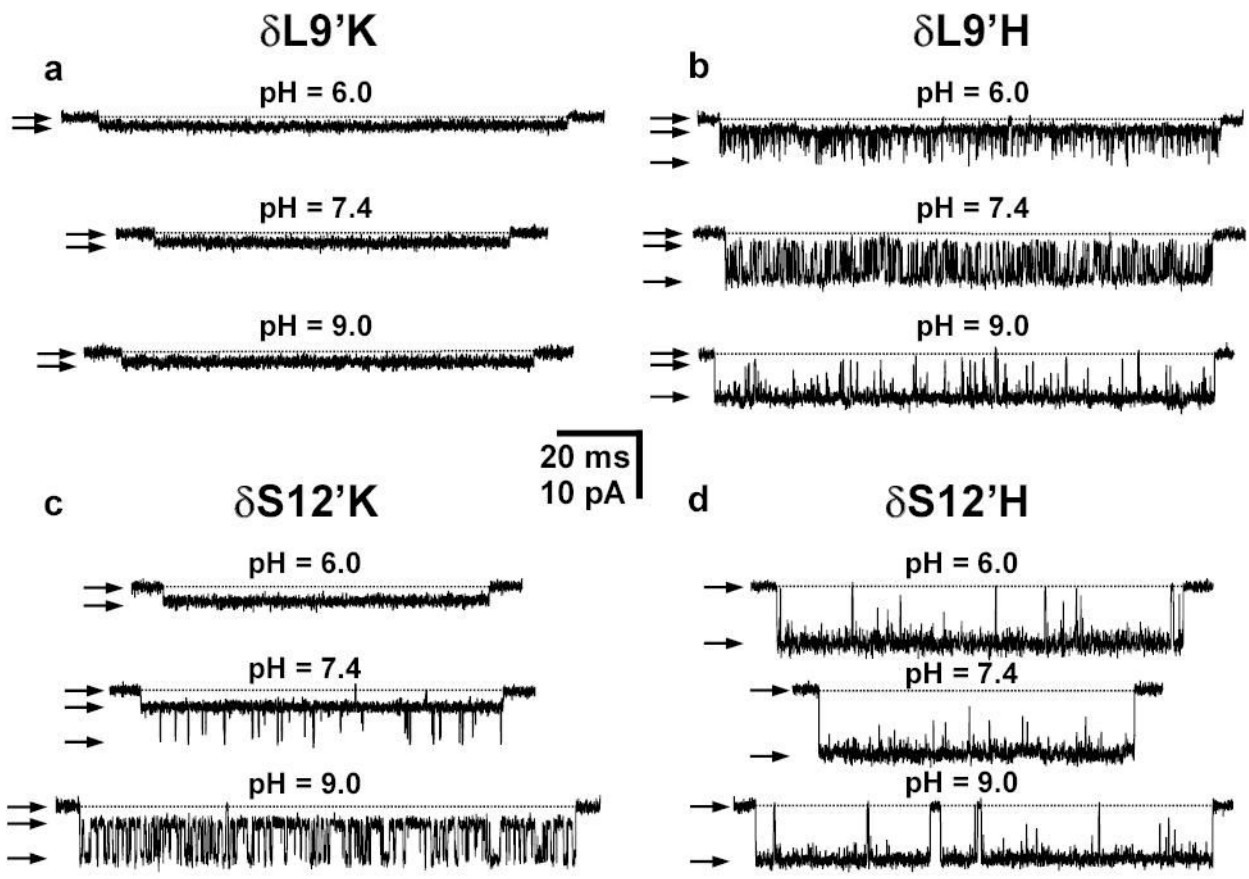

Figure 3. pH-dependence of proton-transfer reactions

a, **b,** Example single-channel inward currents (V ≅ −100 mV, [ACh] = 1 μM) recorded from Leu-to-Lys (**a**) and Leu-to-His (**b**) δ9' mutants at three different pH-values. The microenvironment around δ9' slightly stabilizes the positive εNH_3^+ charge relative to bulk, and thus a lysine remains protonated in the 6.0 – 9.0 pH range. Hence, a histidine, with a lower proton affinity, is needed to reveal this position's ΔpK_a. As expected, the deprotonated state of the histidine is favored as the pH increases. **c**, **d,** Example single-channel inward currents (V ≅ −100 mV, [ACh] = 1 μM) recorded from Ser-to-Lys (**c**) and Ser-to-His (**d**) δ12' mutants at three different pH-values. The microenvironment around δ12' destabilizes the positive charge relative to bulk, and thus a histidine remains deprotonated in the 6.0 – 9.0 pH range. An arginine at this position, in contrast, still retains the labile proton, even at pH = 9.0 (data not shown). Thus, only a lysine, with an intermediate proton affinity, can reveal the ΔpK_a at δ12'. As expected, the deprotonated state of the lysine is favored as the pH increases. Openings are downwards. The shut and the two open current-levels are indicated by arrows. The shut level is also indicated by a horizontal dotted line. Display f_c = 6 kHz.

Table 1

Position-dependence of rates of proton transfer and pK_as at −100 mV

Probed position	Mutation	pH	Deprotonation rate (s^{-1})	Protonation rate (s^{-1})	pK_a, pore	ΔpK_a	Intervals	No.
δ -4’	C → H*	7.4	5,892 ± 1,162	2,859 ± 549	7.09 ± 0.003	+0.69	119,772	2
δ -2’	G → H*	7.4	2,913 ± 140	26,540 ± 2,339	8.36 ± 0.06	+1.96	111,715	2
δ -1’	E → H*	7.4	16,257 ± 15	1,063 ± 17	6.22 ± 0.008	−0.18	52,660	2
δ 0’	K → A, R	6.0	--	--	<5.0†	< −7.00	--	--
δ 1’	T → K*	7.4	413 ± 32	4,252 ± 462	8.41 ± 0.08	−1.99	74,559	6
δ 2’	S → H*	7.4	5,537 ± 87	3,126 ± 56	7.15 ± 0.01	+0.75	111,071	2
δ 3’	V → K	6.0	18,045 ± 937	2,434 ± 138	5.13 ± 0.005	−5.27	32,384	4
δ 4’	A → R	6.0	--	--	<5.0†	< −7.00	--	--
δ 5’	I → H	7.4	15,829 ± 620	3,331 ± 105	6.72 ± 0.003	+0.32	48,977	2
δ 6’	S → H*	7.4	7,499 ± 297	5,970 ± 104	7.30 ± 0.01	+0.90	549,337	3
δ 7’	V → K	6.0	12,726 ± 18	4,068 ± 44	5.50 ± 0.005	−4.90	15,155	2
δ 8’	L → K	7.4	740 ± 80	160 ± 9	6.74 ± 0.05	−3.66	66,552	3
δ 9’	L → H	7.4	7,217 ± 141	3,646 ± 108	7.10 ± 0.004	+0.70	465,715	2
δ 10’	A → K	7.4	1,792 ± 77	2,383 ± 63	7.53 ± 0.01	−2.87	155,089	8
δ 11’	Q → K*	6.0	85 ± 7	16 ± 1	5.27 ± 0.02	−5.13	12,473	2
δ 12’	S → K	7.4	443 ± 11	13,028 ± 345	8.87 ± 0.008	−1.53	69,745	4
δ 13’	V → H	7.4	19,102 ± 422	3,655 ± 294	6.68 ± 0.03	+0.28	541,227	3
δ 14’	F → K	7.4	1,799 ± 90	395 ± 12	6.74 ± 0.03	−3.66	41,793	4
δ 15’	L → H	6.0	8,173 ± 518	3,835 ± 314	5.67 ± 0.008	−0.73	15,245	2
δ 16’	L → H	6.0	--	--	6.7‡	+0.30	--	--
δ 17’	L → H	6.0	--	--	6.4‡	0	--	--

pH: pH-value used in the calculation of the pK_a. At several positions, proton-transfer events were clearly resolved only at pH = 6.0 (in the pipette). Although pK_as turned out to be somewhat pH-dependent (data not shown), the deviations from their values at pH = 7.4 are expected to be small. ΔpK_a: pK_a, pore - p$K_{a,\ bulk}$. Intervals: total number of idealized intervals used for kinetic analysis. No.: number of independent patches. Standard errors and means were calculated from the means of individual patches.

*AChRs bearing these δ-subunit mutations also contained the T264P mutation in the non-adjacent ε subunit (M2 ε 12’ position). This mutation prolongs individual activations of the channel[42] and, thus, increases the number of main-level ⇌ sublevel transitions recorded.

†pK_a-values estimated qualitatively on the basis of the finding that arginines engineered at these positions appear to be completely deprotonated, even at pH = 6.0.

‡Although protonation/deprotonation of histidines engineered at these positions was evident from the electrophysiological recordings, the individual transitions could not be resolved reliably. Thus, these pK_a-values are qualitative estimates made on the basis of a comparison with the appearance of recordings from the other constructs.